Scripta Materialia 194 (2021) 113679

Contents lists available at ScienceDirect

Scripta Materialia

journal homepage: www.elsevier.com/locate/scriptamat

On the geometric trajectories of pores during the thermal sintering of relevant catalyst supports

Valeriya Zarubina[a,b], Ignacio Melián-Cabrera[c,*]

[a] Erasmus University Rotterdam, Erasmus University College (EUC), Nieuwemarkt 1A, HP Rotterdam 3011, The Netherlands
[b] Faculty of Science and Engineering, University of Groningen, Nijenborgh 4, AG Groningen 9747, The Netherlands
[c] Applied Photochemistry and Materials for Energy Group, University of La Laguna, Avda. Astrofísico Francisco Sánchez, s/n, PO BOX 456, 38200 San Cristóbal de La Laguna, S/C de Tenerife, Spain

ARTICLE INFO

Article history:
Received 4 December 2020
Accepted 16 December 2020
Available online 26 December 2020

Keywords:
Alumina
Coarsening
High-resolution sorption analysis
Mesoporous materials
Silica
Sintering
Thermal treatment

ABSTRACT

The thermal events typically encountered during the reactivation of inorganic catalytic supports have been investigated. For this, two relevant inorganic materials were studied; an amorphous silica and a gamma (γ) alumina. The materials were thermally treated in air at temperatures ranging 700 up to 1100 °C and the structural and textural changes were assessed. The crystallinity was enhanced and the textural parameters decreased, but the most remarkable effect was the pore trajectory. This varies depending on the sintering mechanism, contractive sintering (silica) or coarsening (alumina), which was detected by high-resolution physisorption. The reduction in the surface area is not a good indicator of the pore changes; in addition to pore changes, the material can also suffer densification, and both effects determine the surface area. Finally, the study shows that thermal treatment is an easy way to modify the pore size of the studied materials; the γ-alumina showing more controllability.

Catalysis can be found almost everywhere, from the human body up to industrial processes; both scale and environment vary hugely. Heterogeneous catalysis involves the application of solid materials that act as catalysts; they enable the production of clean fuels, many chemicals, purify water and mitigate hazardous emissions to the environment [1,2]. The variety of heterogeneous catalysts ranges from bulk materials, aggregates, metal clusters, non-structured to structured porous materials and supported counterparts. One group of heterogeneous catalysts refers to supported catalysts [3,4], meaning that the active component is deposited onto a thermostable organic or inorganic material. Examples are Pd/Al_2O_3 for methane combustion [5,6], Pt/Al_2O_3 for CO oxidation [7,8], $Rh\text{-}Re/SiO_2$ for hydrogenolysis of tetrahydrofurfuryl alcohol [9] or renewable caprolactone [10], to site a few. However, non-metals can also be deposited [11]. In some cases, the inorganic material is active by itself [12,13], as shown for the oxidative hydrogenation of ethylbenzene.

Most of these processes require reactivation of the catalyst due to the deposition of carbonaceous moieties during reaction. For this, calcination is applied at high temperatures using air. This process is able to oxidize such carbon deposits by combustion. Though recent studies have shown the feasibility of non-thermal methods [14–17], calcination is still the first choice though it is an energy-intensive process. One of the key issues during such oxidative reactivation is that hot-spots can occur [18], meaning that the temperature can be locally high. Therefore, the catalyst is exposed to temperatures that can be detrimental from the metal dispersion or inorganic support's structure and texture point of view. The effect of oxidative conditions on supported-metal catalysts has been widely studied [19,20]. An area that has received less attention is the inorganic support's side; i.e. what is the effect of high temperatures on the inorganic support. A point of concern is if such inorganic materials can suffer irreversible changes both on structure and texture. The motivation of this work is therefore to investigate the changes of relevant catalyst supports, silica and alumina, upon high-temperature treatments. Such treatments aim to emulate the local hot-spots. To support the results, theoretical models from ceramic thermal sintering were considered. It was surprisingly found that the geometric trajectory of the pores upon high-temperature treatments is not an obvious phenomenon.

As starting materials, two inorganic supports were investigated; a low-SiO_2 stabilized γ-Al_2O_3 extrudates (Albemarle Catalysts BV, denoted as ALU) and an amorphous silica (61138, Saint-Gobain NorPro, denoted as AS). The extrudates were crushed and sieved into a 212-425 μm fraction, which was used for the thermal treatment experiments. Each material was thermally treated at temperatures of 700, 900 and 1100 °C in ceramic crucibles, using a box

* Corresponding author.
E-mail address: ignacio.melian.cabrera@ull.edu.es (I. Melián-Cabrera).

https://doi.org/10.1016/j.scriptamat.2020.113679
1359-6462/

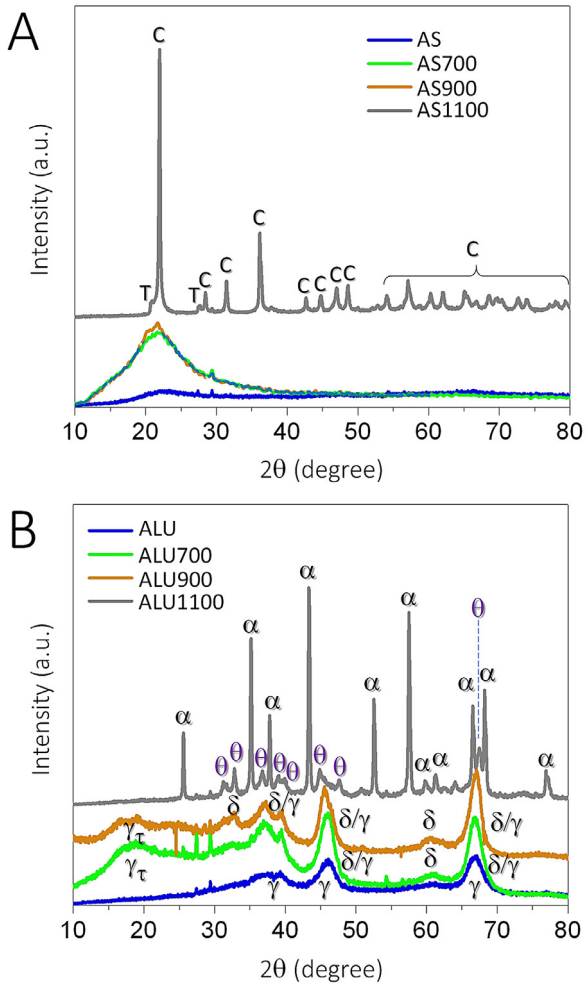

Fig. 1. Experimental XRD patterns for the silica (A) and alumina materials (B). The phase assignments correspond to: C (cristobalite), T (tridymite), γ (gamma alumina), γ_τ (tetragonal gamma alumina), δ (delta alumina), θ (theta alumina) and α (alpha alumina).

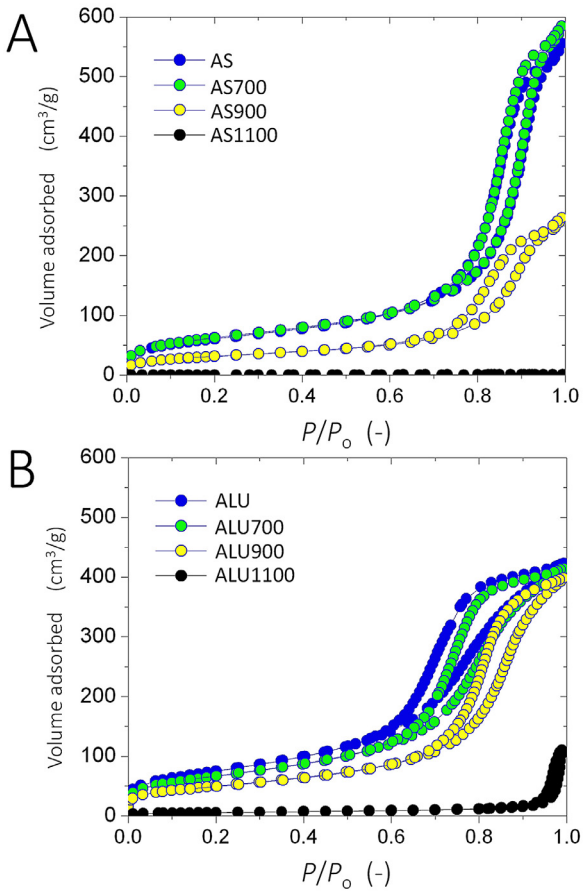

Fig. 2. Nitrogen sorption isotherms of the silica (A) and alumina materials (B).

furnace in static air at a rate of 4 °C/min and held for 8 h in a shallow-bed configuration. The resulting materials were labelled as ALUX00 (alumina materials) or ASX00 (silica materials), where X00 corresponds to the treatment temperature in degree Celsius. Additional experimental information can be found in the Electronic Supporting Information.

We will first describe the results for the silica, and after that, the alumina's section will be discussed. Ultimately, both systems will be compared and a preliminary phenomenological interpretation will be given.

The silica materials were first evaluated by XRD analysis. Structurally, the bare silica consists of an amorphous phase (AS in Fig. 1A) displaying a broad reflection at ~22 degree. Upon thermal treatment at 700 and 900 °C, the material remains amorphous though the reflection at 22 degree becomes more pronounced. It is only at 1100 °C when the material suffers a significant structural modification, with the appearance of crystalline phases. The reflections were indexed to the cristobalite (JCPDS 39-1425) mainly, with a minor contribution of tridymite (JCPDS 42-1401). This assignment agrees well with Zimmerman et al [21], who indexed both phases. Sometimes the tridymite phase is not indexed despite it has a different crystal structure and well-defined reflections, as an example in [22]. The textural features were evaluated by N_2 physisorption (Fig. 2A). The bare silica shows an isotherm type IV with hysteresis H1, representing solids with cylindrical pore geometry – cylindrical, though the pores can be tortuous – with relatively high pore size uniformity and facile pore connectivity [23]; so they do not possess restrictions. Upon thermal treatment, the isotherms do not change their shape remaining type IV-H1 (Fig. 2A), with the exception of AS1100 which does not adsorb much (nearly flat isotherm). The porosity of these materials (AS, AS700 and AS900) originates from the interparticle space of spherical or spheroidal domains. The surface area decreases with the applied temperature as can be seen in Fig. 3A, though at 700 °C it does not change much with the major changes at 900 and 1100 °C (52 and 99% with respect to the AS). In the case of AS1100, the experimentally determined S_{BET} was below 1 m^2/g due to the high crystallinity of the material obtained upon the thermal treatment.

The alumina materials were also evaluated by XRD analysis (Fig. 1B). The bare alumina corresponds to a gamma (γ) alumina (JCPDS 10-0425) [24], which is formed by rather broad bands. The thermal treatment produces some changes in the XRD patterns at 700 and 900 °C, with the appearance of new reflections associated to δ-alumina (JCPDS 46–1131). However, the pattern cannot be assigned to a pure alumina phase but to a mixture of γ and δ phases. At 700 °C, γ-alumina seems to be the dominant phase, by qualitative inspection, whereas at 900 °C the dominant phase is δ-alumina. Such a complexity in phase identification for the alumina has been reported by many groups, among others Boumaza et al as an example [24]. Grzybek et al [25] applied a Rietveld refinement method and were able to detect a tetragonal gamma alumina, which is indicated in Fig. 1B as γ_τ. When the temperature was increased up to 1100 °C, the changes in crystallinity were

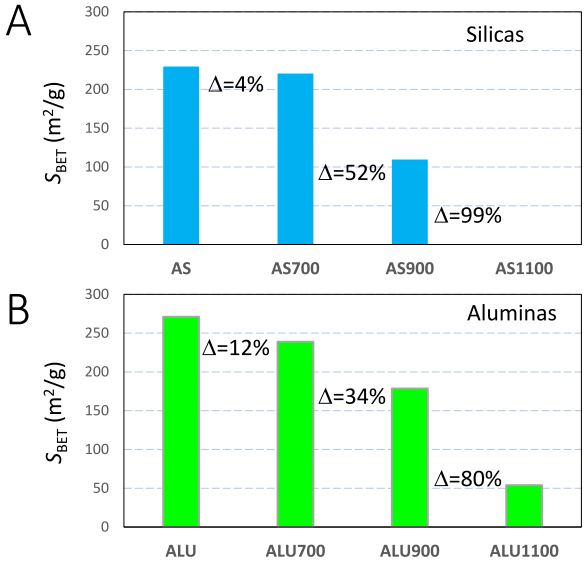

Fig. 3. Evolution of the BET surface area of the silica (A) and alumina materials (B), upon the thermal treatments.

Table 1
Experimentally observed changes upon thermal treatment (700-1100 °C) of two relevant catalytic inorganic supports.[a]

Material	Crystallinity	Porosity (S_{BET})	Pore size
Silica	Increases	Decreases	Reduces
Alumina	Increases	Decreases	Enlarges

[a] Note that these trends correspond to the studied materials.

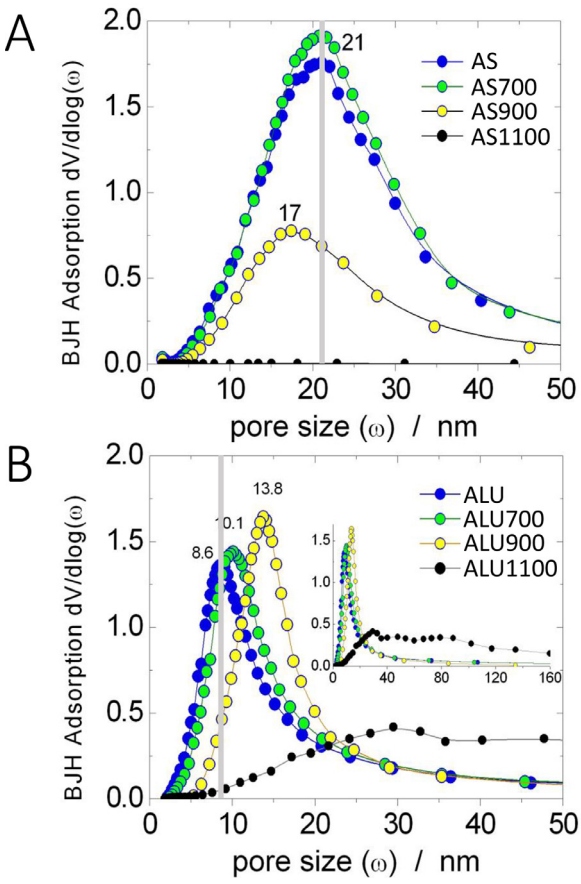

Fig. 4. High-resolution BJH pore size distributions derived from N_2 adsorption data of the silica (A) and alumina materials (B).

more obvious with the presence of θ-alumina (JCPDS 35–0121) and α-alumina (JCPDS 42–1468) as main phases. The narrow nature of the reflections indicates the high crystallinity of the phases. A similar effect occurred for the silica, where very crystalline cristobalite and tridymite appeared at 1100 °C. The textural changes were assessed by N_2 physisorption (Fig. 2B). The bare alumina shows an isotherm type IV with hysteresis H1, as was also observed for the bare silica, with good pore connectivity and no restrictions [23]. The total adsorption capacity of the bare alumina is smaller than for the silica with a plateau at ca. 400 cm^3/g whereas the silica shows it at ca. 550 cm^3/g. Upon thermal treatment, the isotherm does not change its shape remaining type IV-H1. The porosity of these alumina-based materials also originates from the interparticle space. The surface area is reduced with the applied temperature as shown in Fig. 3B, but less severe compared to the silica. In the case of ALU1100, the experimentally determined S_{BET} was still considerable, with a value of ca. 50 m^2/g.

The structural and textural changes observed upon the thermal treatments for both materials have been summarised in Table 1. Since the porosity is interparticle – i.e. formed by the interspace between the aggregates – the higher the crystallinity (larger crystals) the lower the surface area; the space between large particles corresponds to large pores, and therefore a low surface area is obtained. This is seen in Table 1 for both systems; as the crystallinity increases, the surface area decreases. This is a general observation that can be found for many other inorganic systems. However, there is an aspect that is less obvious. It regards the pore size; does it decrease or increase? And if it decreases, how can we explain the lower surface area, as smaller pore sizes are expected to have a higher surface area? This will be rationalised in the next sections.

To understand this aspect better, we looked at the high-resolution pore size distributions (PSD) for both systems, derived from the N_2 sorption data. These are represented in Fig. 4. For the silica (Fig. 4A), the starting material shows a pore size centered at around 21 nm. Such a value agrees well with the geometric average value (Table 1 in Electronic Supporting Information), considering that BJH provides an overestimation [26]. At 700 °C, the PSD remains at 21 nm, thus it seems that the pore structure is resistant to change. This agrees well with the BET surface area which is very similar to the AS case (4% variation only). This can be related to the thermal history of the AS silica material that could have been treated at temperatures around 700 °C. At 900 °C, the PSD is flattened and the maximum shifts towards 17 nm. The geometrical pore size also shows the same trend (Table 1 in Electronic Supporting Information). At 1100 °C, the PSD is fully flat at nil; the pore volume is below 0.005 cm^3/g and the BET surface area is below 1 m^2/g. That means that the material has been sintered, becoming a continuous solid phase with only some residual porosity. Sintering is a well-known phenomenon that takes place below the melting point and is used in e.g. moulding to create different kinds of micro- to macro-scale pieces. The textural data evidence that the silica, upon thermal treatment, undergoes a pore contraction until the porosity – using N_2 as probe molecule – disappears. This phenomenon can be explained due to the system having a high particle coordination. When having a high number of contact points, sintering is favoured rendering a system with a lower void space. This can be seen in Table 2 with the mechanism denoted as contractive sintering. Such a mechanism was deduced from German [27], who provided theoretical basis for the pore reduction and pore expansion during sintering.

This finding of pore contraction in the silicas, makes the interpretation of the surface area's reduction non trivial. One would ex-

Table 2
Interpretation of the pore trajectories upon thermal treatment by sintering of inorganic materials having interparticle porosity. To highlight the concept, spherical particles were employed.

Mechanism	Particle coordination	Pore trajectory	Model[b]	Effect of surface area
Contractive sintering[a]	High	Contraction		Surface area (m^2/g) decreases despite the pores are smaller due to the density increase, i.e. more mass per unit of volume.
Coarsening	Low	Expansion	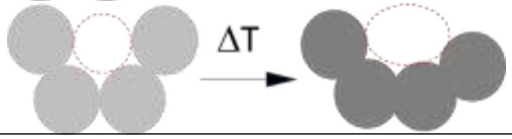	Surface area (m^2/g) decreases due to larger pores and density increase, i.e. more mass per unit of volume.

[a] This term is often found in literature as 'densification' meaning that the change in porosity with sintering divided by the starting porosity [27]. However, it can get confused with the more conventional term for density. For both mechanisms, the density increases.
[b] The contraction in volume due to density changes has not been considered in these models, for simplicity, due to the fact that the density was not analysed.

pect that smaller pores in AS900 would render a higher surface area, whilst the opposite was found; a lower surface area than AS and AS700, while those materials possess larger pores. The reason for this is that there seem to be two opposing effects: pore size and density. The pores are smaller but the material density changes; it increases with temperature based on experimental evidence [27]. Therefore, such a density increase dominates the BET surface area parameters. The overall interpretation of the silica systems (see model in Table 2) is that a high particle coordination during the thermal treatment favours the contractive sintering, with a contraction of the pores until the almost-complete removal of the porosity. The density increase seems to dominate the BET values.

The PSDs for the alumina materials are given in Fig. 4B. The starting material shows a pore size centered at around 8.6 nm. Such a value agrees well with the geometric average value (Table 1 in Electronic Supporting Information). Upon thermal treatment, the PSD moves towards larger pores, 10.1 nm (ALU700), 13.8 nm (ALU900) and ~30 nm with a broad shoulder (ALU1100). The effect is just the opposite to the silica's behaviour. Here, the lower BET surface area is due to the larger pores but also to the density increase. In general, regardless the material suffers contractive sintering or coarsening, the density increases with the treatment temperature [27].

The interpretation of the alumina systems (see model in Table 2) considers that having a low particle coordination during the thermal treatment favours the coarsening, with a pore expansion and the formation of a chain-like structure. Such a phenomenon was observed for other alumina systems by López-Pérez et al [28] where the pore size distributions could be rationalised by the mesophase particle morphology; those mesophases having an heterogenous shape (i.e. low particle coordination) favouring the coarsening of the pores, resulted in a broad PSD. However, it must be stressed that López-Pérez et al [28] rationalised the PSD of the aluminas, from various synthesis approaches, whilst temperature was maintained constant, so it is a different approach than this study.

This rationalization is a preliminary interpretation and other effects should not be ruled out yet. For instance, the presence of internal gas from the decomposition (dehydroxylation in the case of the oxides) or the presence of additives can change the sintering process. German [27] indicated that additives modify the grain growth during sintering; some additives retard grain growth, whilst others accelerate it. As the alumina employed in this study was promoted with silica (1 wt. %), the effect of silica should not be ruled out as playing a role in the pore expansion as well.

As a conclusion, two relevant inorganic catalytic materials were studied in relation to high-temperature treatments. The crystallinity was enhanced with the formation of new phases and the textural features decreased, for both materials. However, the pore size trajectory behaved differently, depending on the sintering mechanism. The main conclusion of this preliminary study is that the pore trajectory, during thermal treatment for these inorganic materials, can display a contractive sintering (pore contraction) or a coarsening effect (pore expansion), depending on the dominating mechanism. Such information can only be obtained by high-resolution textural analysis. The reduction of the S_{BET}, a typical shortcut approach, is not a good indicator of pore expansion, as shown in this study. From a practical point of view, this study shows that thermal treatment is an easy way to modify the pore size of the studied materials, where γ-alumina shows more controllability.

Declaration of Competing Interest

The authors declare that they have no known competing financial interests or personal relationships that could have appeared to influence the work reported in this paper.

Acknowledgement

This research was also co-financed by the NWO Vidi grant no. 10284 and the Dutch Technology Foundation STW (STW07983).

Supplementary materials

Supplementary material associated with this article can be found, in the online version, at doi:10.1016/j.scriptamat.2020.113679.

References

[1] J. Hagen, Industrial Catalysis: a Practical Approach, Wiley-VCH Verlag GmbH, Weinheim, 2015.
[2] J.A. Moulijn, M. Makkee, A.E. van Diepen, Chemical Process Technology, second ed., Wiley-VCH, Chichester, 2013.
[3] P. Munnik, P.E. de Jongh, K.P. de Jong, Chem. Rev. 115 (2015) 6687–6718.
[4] O.S. Alexeev, B.C. Gates, Ind. Eng. Chem. Res. 42 (2003) 1571–1587.
[5] R. Burch, P.K. Loader, Appl. Catal. B 5 (1994) 149–164.
[6] K. Murata, J. Ohyama, Y. Yamamoto, S. Arai, A. Satsuma, ACS Catal. 10 (2020) 8149–8156.
[7] S.H. Oh, R.M. Sinkevitch, J. Catal. 142 (1993) 254–262.
[8] A. Beniya, S. Higashi, N. Ohba, R. Jinnouchi, H. Hirata, Y. Watanabe, Nat. Commun. 11 (2020) 1888.
[9] S. Koso, I. Furikado, A. Shimao, T. Miyazawa, K. Kunimori, K. Tomishige, Chem. Commun. (2009) 2035–2037.

[10] T. Buntara, S. Noel, P.H. Phua, I. Melián-Cabrera, J.G. de Vries, H.J. Heeres, Angew. Chem. Int. Ed. 50 (2011) 7083–7087.
[11] V. Zarubina, H. Talebi, H. Jansma, K. Góra-Marek, C. Nederlof, F. Kapteijn, M. Makkee, I. Melián-Cabrera, Appl. Catal. A 514 (2016) 173–181.
[12] V. Zarubina, C. Nederlof, B. van der Linden, F. Kapteijn, H.J. Heeres, M. Makkee, I. Melián-Cabrera, J. Mol. Catal. A 381 (2014) 179–187.
[13] I. Melián-Cabrera, V. Zarubina, C. Nederlof, F. Kapteijn, M. Makkee, Catal. Sci. Technol. 8 (2018) 3733–3736.
[14] S. Khangkham, C. Julcour-Lebigue, S. Damronglerd, C. Ngamcharussrivichai, M.H. Maneroa, H. Delmas, Appl. Catal. B 140–141 (2013) 396–405.
[15] L.Y. Jia, Al Farouha, L. Pinard, S. Hedan, J.-D. Comparot, A. Dufour, K.B. Tayeb, H. Vezin, C. Batiot-Dupeyrat, Appl. Catal. B 219 (2017) 82–91.
[16] M.V. Morales, K. Góra-Marek, H. Musch, A. Pineda, B. Murray, S. Stefanidis, L. Falco, K. Tarach, E. Ponomareva, J.H. Marsman, I. Melián-Cabrera, Appl. Catal. A 562 (2018) 215–222.
[17] E. Ponomareva, M.A. López-Martínez, D. Wigger, M.V. Morales, I. Melián-Cabrera, Appl. Catal. A 569 (2019) 134–140.
[18] L. López Pérez, M.J. Ortiz-Iniesta, H.J. Heeres, I. Melián-Cabrera, Mater. Lett. 118 (2014) 51–54.
[19] J.G. McCarty, G. Malukhin, D.M. Poojary, A.K. Datye, Q. Xu, J. Phys. Chem. B 109 (2005) 2387–2391.
[20] Q. Xu, K.C. Kharas, B.J. Croley, A.K. Datye, Top. Catal. 55 (2012) 78–83.
[21] A.B. Zimmerman, A.M. Nelson, E.G. Gillan, Chem. Mater. 24 (2012) 4301–4310.
[22] S.H. Xue, H. Xie, H. Ping, Q.C. Li, B.L. Su, Z.Y. Fu, RSC Adv. 5 (2015) 71844–71848.
[23] M. Kruk, M. Jaroniec, Chem. Mater. 13 (2001) 3169–3183.
[24] A. Boumaza, L. Favaro, J. Lédion, G. Sattonnay, J.B. Brubach, P. Berthet, A.M. Huntz, P. Roy, R. Tétot, J. Solid State Chem. 182 (2009) 1171–1176.
[25] G. Grzybek, K. Ciura, S. Wójcik, J. Gryboś, P. Indyka, M. Inger, K. Antoniak-Jurak, P. Kowalik, A. Kotarba, Z. Sojka, Catal. Sci. Technol. 7 (2017) 5723–5732.
[26] S. Lowell, J.E. Shields, M.A. Thomas, M. Thommes, Characterization of Porous Solids and Powders: Surface Area, Pore Size and Density, Springer, Dordrecht, 2004.
[27] R.M. German, Sintering: from Empirical Observations to Scientific Principles, Elsevier, Oxford, 2014.
[28] L. López Pérez, S. Perdriau, G. ten Brink, B.J. Kooi, H.J. Heeres, I. Melián-Cabrera, Chem. Mater. 25 (2013) 848–855.